THE JOURNAL OF PHYSICAL CHEMISTRY Letters

Letter

pubs.acs.org/JPCL

Modulating Exciton Dynamics in Composite Nanocrystals for Excitonic Solar Cells

Isabella Concina

Dipartimento di Ingegneria dell'Informazione, Università di Brescia, Via Valotti 9, 25133 Brescia, Italy

Cristian Manzoni

Istituto di Fotonica e Nanotecnologie (IFN)-CNR, Politecnico di Milano, Piazza Leonardo da Vinci 32, 20133 Milano, Italy

Giulia Grancini

Center for Nano Science and Technology@Polimi, Istituto Italiano di Tecnologia, via Giovanni Pascoli 70/3, 20133, Milan, Italy

Mert Celikin, Afsoon Soudi, and Federico Rosei

INRS Centre for Energy, Materials and Telecommunications, 1650 Boulevard Lionel Boulet, J3X 1S2 Varennes, Quebec, Canada

Margherita Zavelani-Rossi and Giulio Cerullo

Dipartimento di Fisica, Politecnico di Milano, Istituto di Fotonica e Nanotecnologie (IFN)-CNR, Piazza Leonardo da Vinci 32, 20133 Milano, Italy

Alberto Vomiero*

SENSOR Lab, Istituto Nazionale di Ottica, CNR, Via Branze 45, 25123 Brescia, Italy

Luleå University of Technology, 971 98 Luleå, Sweden

Supporting Information

ABSTRACT: Quantum dots (QDs) represent one of the most promising materials for third-generation solar cells due to their potential to boost the photoconversion efficiency beyond the Shockley–Queisser limit. Composite nanocrystals can challenge the current scenario by combining broad spectral response and tailored energy levels to favor charge extraction and reduce energy and charge recombination. We synthesized PbS/CdS QDs with different compositions at the surface of TiO_2 nanoparticles assembled in a mesoporous film. The ultrafast photoinduced dynamics and the charge injection processes were investigated by pump–probe spectroscopy. We demonstrated good injection of photogenerated electrons from QDs to TiO_2 in the PbS/CdS blend and used the QDs to fabricate solar cells. The fine-tuning of chemical composition and size of lead and cadmium chalcogenide QDs led to highly efficient PV devices (3% maximum photoconversion efficiency). This combined study paves the way to the full exploitation of QDs in next-generation photovoltaic (PV) devices.

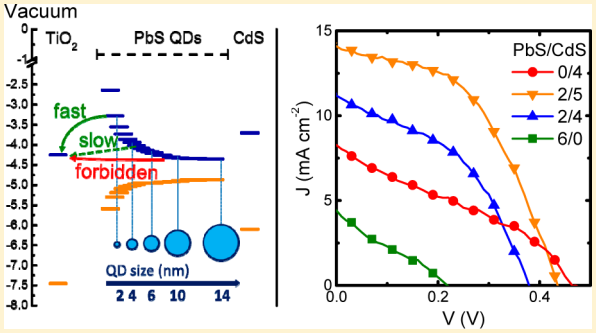

Quantum dot solar cells (QDSCs) are emerging as a viable solution to boost the photoconversion efficiency (PCE) beyond the Shockley–Queisser limit.[1] In these devices, the PCE is ultimately determined by the processes of solar light absorption and exciton/charge interconversion.[2−4] Recently, lead chalcogenides (mainly lead sulfide (PbS) and selenide (PbSe)) have been used in QDSCs to enhance solar light absorption in the infrared region, which is typically dissipated in the form of heat in traditional silicon-based solar cells; however,

Received: April 12, 2015
Accepted: June 8, 2015
Published: June 8, 2015

DOI: 10.1021/acs.jpclett.5b00765
J. Phys. Chem. Lett. 2015, 6, 2489–2495

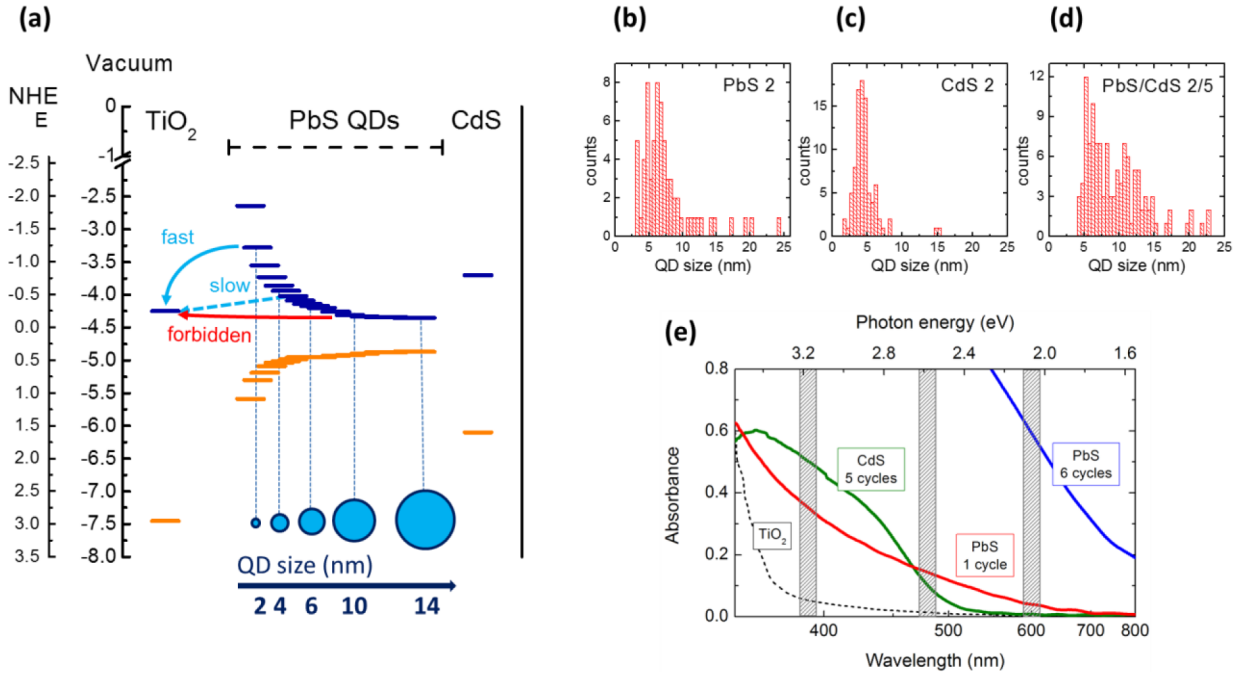

Figure 1. (a) Scheme of electronic band alignment for bulk TiO_2, bulk CdS and PbS QDs of different size for diameter ranging from 1 to 14 nm. The energy levels for PbS QDs are calculated according to ref 4. Electron injection paths from PbS QDs to the oxide are indicated by arrows (solid azure: fast injection; dash azure: slow injection: solid red: injection prohibited). (b–d) Size distribution of QDs grown through the SILAR technique measured from AFM on a highly ordered pyrolitic graphite (HOPG) substrate: (b) PbS, 2 cycles; (c) CdS, 2 cycles; (d) PbS/CdS 2/5 cycles. (e) UV–vis absorption spectra of CdS QDs (green solid line) and PbS QDs for different QD sizes (increasing from red to blue), together with the absorption spectrum of TiO_2 and the indication of the pump spectra (dashed rectangles) used in the differential transmission measurements.

unfavorable electronic band alignment prevents efficient charge separation and transfer to the semiconducting oxide, which acts as an electron transporter.[4−6] It has been recently demonstrated that lead-based colloidal QDs are able to transfer hot electrons produced by absorption of energetic photons to TiO_2 before electron cooling takes place,[3,7] leading to efficient transfer of the excitation to the oxide scaffold. This mechanism however is still highly debated. Other recent works report the lack of hot electron injection from PbSe QDs to nanocrystalline thin films[8] and the slow electron transfer in colloidal PbS QDs linked to TiO_2 nanoparticles.[4,9] In this respect, the adoption of composite nanocrystals can combine broad spectral response and proper energy level alignment to favor efficient charge extraction and reduce charge and energy losses under operating conditions. Composite nanocrystals based on lead chalcogenides allow an enhanced PCE[10] with broad-band optical absorption while preserving a suitable electronic structure for electron injection at the interface with the metal oxide used as an electron-transport material. Core–shell PbS/CdS QDs synthesized by the hot injection method were very recently successfully used in QDSCs.[11]

In a particular configuration of QDSCs,[1] QDs are grafted to the surface of the oxide scaffold either directly or through various kinds of ligands. While indirectly linked colloidal QDs exhibit much better defined optical properties in terms of size distribution and excitonic peak, "naked" QDs (i.e., QDs that do not present any surface passivation through capping with organic ligands and that are typically grown directly at the oxide surface) guarantee increased PCE because the direct link to the oxide surface leads to fast exciton dissociation and electron injection.[12,13] Exciton dynamics have been thoroughly investigated in colloidal QDs,[14,15] and different aspects have been considered, such as the role of the size[4] and of the ligands.[9] In particular, it has been shown that reducing the size results in light absorption at higher photon energies and in faster injection of charges to the electrodes due to the upward shift of the conduction band (CB).[4,6,14] In addition, it has been demonstrated that it is possible to shift the energy level alignment between CdS QDs and TiO_2 using molecular dipoles and thus influence electron injection into the electrode.[16] Naked QDs on oxides, on the contrary, have been rarely studied, and only one report exists on their photophysics in a limited spectral interval (900–1200 nm).[13] Nevertheless, the PCE that these materials exhibit, above 5%,[12,13] calls for a more in-depth investigation on the influence of their physical and chemical characteristics on the photoexcitation dynamics. This is particularly challenging because naked QDs typically exhibit a broad size distribution, leading to the simultaneous presence of a distribution of quantized systems and different exciton dynamics, which cannot be easily disentangled.

Time-resolved optical spectroscopies are a very powerful tool to investigate exciton dynamics and, in general, the processes related to photoinduced exciton generation and dissociation and charge injection in composite systems.[6,14,17] They are particularly relevant because charge generation dynamics are intimately connected to the PCE of an operating device. For this reason, the combined investigation of the ultrafast optical response and functional characterization of solar cells allows one to correlate the fundamental physical/chemical processes that occur in the operating device and the light-to-electric power conversion.

Here, we study composite QDs formed by lead and cadmium chalcogenides directly grafted on a titanium oxide surface through the successive ionic layer absorption and reaction (SILAR) technique.[18−20] We focus on systems with QDs of different size and composition: PbS, CdS, and mixed PbS/CdS.

DOI: 10.1021/acs.jpclett.5b00765
J. Phys. Chem. Lett. 2015, 6, 2489−2495

We measure, by means of femtosecond pump−probe spectroscopy, the ultrafast dynamics of the photogenerated species and provide a rationale to understand the fundamental processes, which take place in QDs−oxide systems. We demonstrate that exciton dissociation dynamics can be finely tuned by modulating the electronic band alignment between the QDs and the oxide. Finally, we characterize working solar cells based on composite QDs by providing a straightforward methodology for a rational design of high-efficiency QDSCs.[10,21−24]

The position of the energy levels of the QDs depends on their composition and size. Figure 1a shows the energy diagram of PbS QDs as a function of the dot size, together with that of bulk TiO_2 and bulk CdS. The PbS QD levels are calculated using bulk parameters with energy bands properly scaled according to the effective masses, following ref 4. We plot the results obtained for 13 different dot diameters, ranging from 1 to 14 nm. Because the injection rate of electrons from one medium to another is determined by the band alignment, it appears that the injection from PbS QDs to TiO_2 is unfavored for dots with a diameter larger than 4.3 nm.[4] However, even in this case, injection might occur from hot excitons generated by absorption of high-energy photons that migrate to TiO_2 before thermalization. On the contrary, in the case of CdS, fast electron injection occurs even in bulk form and thus for any size of CdS QDs.

PbS and CdS QDs are grown with varying numbers of SILAR cycles, leading to different dot sizes. The PbS/CdS 2/5 composite system is obtained by first growing two PbS SILAR cycles, followed by five CdS SILAR cycles. In this case, we expect the nucleation of a PbS core directly on the TiO_2 surface, covered by a CdS thin layer. Figure 1b−d displays the size distribution of PbS, CdS, and PbS/CdS dots obtained via atomic force microscopy (AFM) on QDs directly grown on highly ordered pyrolytic graphite substrates. Figure 1e shows the absorption spectra of the QDs used in the solar cells and in the pump−probe experiments, namely, PbS dots obtained by one or six SILAR cycles (PbS1 and PbS6, respectively) or CdS obtained by five cycles, directly grown on a mesoporous transparent TiO_2 thick film. Figure 1e displays also the absorption spectrum of the TiO_2. Transmission electron microscopy (TEM) analysis on QDs is reported in Figure 2. The crystalline lattice of QDs with varying sizes (PbS: (4.3 ± 0.5), CdS: (4.1 ± 0.5), and PbS/CdS: (5.6 ± 0.5) nm) is clearly visible in all samples and consistent with AFM measurements. We carried out energy-dispersive X-ray spectroscopy (EDS) to elucidate the composition of the different crystals and of different areas in the composite system. PbS and CdS QDs present EDS signals coming from Pb and Cd, respectively. EDS analysis conducted on PbS/CdS 2/5 QDs shows the coexistence of both Pb and Cd (Figure 2d). Additionally, Pb-rich (red EDS spectrum in Figure 2d) and Cd-rich regions (black EDS spectrum in Figure 2d) were observed, indicating that the Pb concentration is not homogeneous in this sample. These results are compatible with the formation of an original PbS core surrounded by a thin CdS shell.

To study the ultrafast photoinduced processes in PbS/TiO_2 structures, we first analyzed a reference sample of PbS6 deposited on a glass substrate. We performed pump−probe experiments, with the pump beam photon energy tuned at 600 nm, near the bang gap. The differential transmission ($\Delta T/T$) spectra, reported in Figure S1(a) of the Supporting Information (SI), indicate a nontrivial overlap of different effects.

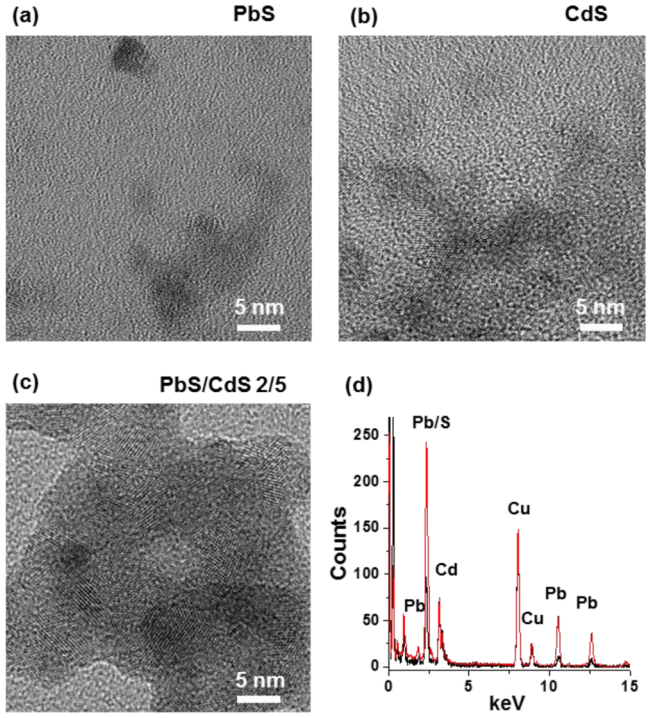

Figure 2. TEM bright field (BF) images of (a) PbS (2 SILAR cycles), (b) CdS (2 cycles), and (c) PbS/CdS (2/5 cycles). The average size of the QDs is (4.3 ± 0.5), (4.1 ± 0.5), and (5.6 ± 0.5) nm, respectively, in very good agreement with AFM measurements. (d) EDS analysis of the PbS/CdS 2/5 composite system, highlighting the presence of Pb, Cd, and S in the sample, as expected. Two different regions are analyzed (black and red spectra, normalized to the intensity of the Cd signal), in which a different Pb/Cd atomic ratio is observed in different regions, in agreement with the hypothesis of a core/shell structure, which results in an inhomogeneous composition. Cu signal comes from TEM copper grids.

Immediately after excitation, a photoinduced absorption (PA) signal appears all over the spectral range, with a peak at around 880−890 nm that can be ascribed to a photoinduced transient Stark effect, associated with a red shift of the absorption spectrum.[25] In about 1 ps, the signal evolves and is dominated by a positive $\Delta T/T$, assigned to carrier photobleaching (PB), which decays on the 10 ps time scale. When the PbS QDs are deposited on a TiO_2 photoanode, the dynamics changes drastically. Figures 3a and 3b show the $\Delta T/T$ spectra of PbS6/TiO_2 (Figure 3a) and PbS1/TiO_2 (Figure 3b), upon excitation at 600 nm. As in the previous case, immediately after excitation (see the trace at 200 fs probe delay), the signal is dominated by PA associated with a transient Stark effect, peaking at around 870−880 nm for both samples; in a few picoseconds, the signal evolves, and PB becomes dominant. The subsequent dynamics is completely different from that measured on the glass substrate. Here, we observe a fast PB recovery and a subsequent new clear PA signal, extending over almost the whole probed region (850−1050 nm). We ascribe this new PA feature to photoinduced absorption of charges in the TiO_2,[26] and we take it as a signature of effective injection at the hybrid PbS QDs/TiO_2 interface.[26] The PA develops very fast, in less than 5 ps (see Figure S1 in the SI), and lives more than 400 ps (see Figure S2 in the SI and the time constants retrieved from the fit), pointing to an efficient charge transfer and the absence of backward transfer. The charge injection appears to be effective with both PbS samples probably because of the size distribution

DOI: 10.1021/acs.jpclett.5b00765
J. Phys. Chem. Lett. 2015, 6, 2489−2495

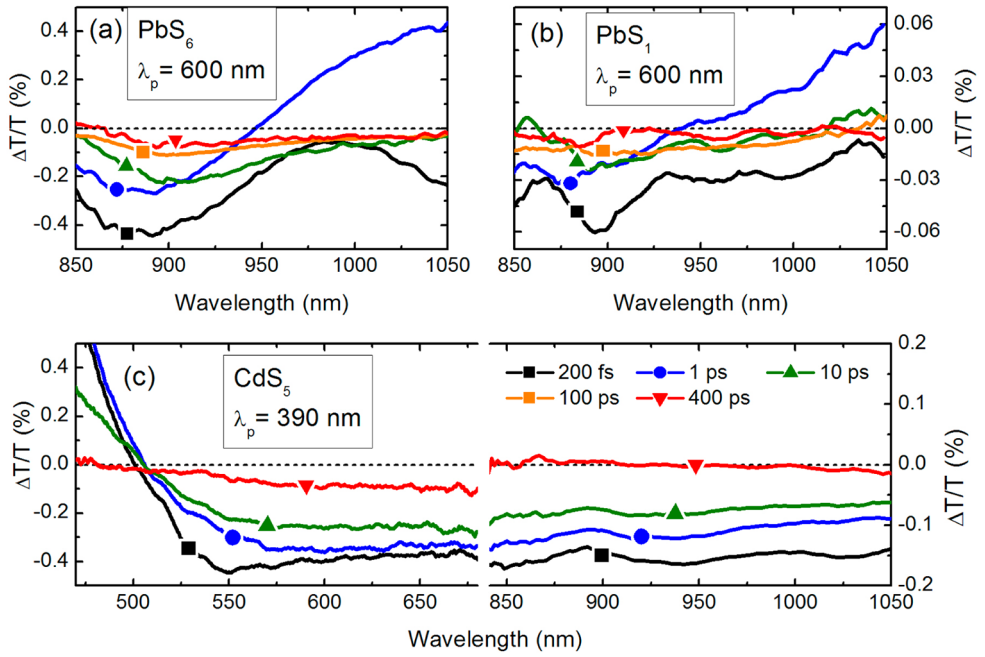

Figure 3. Transient transmission spectra at different time delays of PbS and CdS QDs grown on TiO_2. PbS6 on TiO_2 (a) and PbS1 on TiO_2 (b), after excitation at 600 nm; CdS5 on TiO_2 (c) after excitation at 390 nm.

of the dots, which is quite broad in the SILAR process. Excitation at 600 nm is near the band edge for small dots, leading to immediate direct transfer from the dot to the oxide and providing enough excess energy to larger dots to promote hot electron transfer to the oxide.

Figure 3c shows the $\Delta T/T$ spectral evolution for the sample of CdS QDs, obtained with five SILAR cycles and deposited on TiO_2, pumped at 390 nm and probed over the visible and NIR. PB appears at short wavelengths (λ < 540 nm) due to state filling of the 1S state. At longer wavelengths, we observe a broad-band PA (extending up to 1100 nm). The signal shows a slow decay, completed in hundreds of picoseconds. This PA band can be associated with charge transfer from CdS QDs to the oxide.

After having investigated the photoinduced dynamics of pure CdS QDs deposited on oxide photoanodes, we now consider composite systems of mixed PbS/CdS QDs deposited on TiO_2 as an interesting active compound of high technological relevance for solar cells. The PbS/CdS blend can deliver better performances in terms of absorption spectral coverage and PCE. Figure 4 plots the $\Delta T/T$ spectra after pumping at 480 (Figure 4a) and 600 nm (Figure 4b); these excitation wavelengths were chosen so as to disentangle the various contributions to the $\Delta T/T$ signal; as in the first case, we are exciting both the CdS and the PbS, and in the second case, we excite only the latter one. In both cases, the $\Delta T/T$ spectra are dominated by a broad PA band, extending from the visible to the NIR, which forms in less than 1 ps and has a slow decay. This behavior is similar to the one previously observed on the single type QD samples; therefore, we ascribe it to efficient charge transfer from the QDs to the oxide. In turn, this means that this system is still efficient for charge transfer. In particular, comparing Figure 4a with Figure 3c, it appears that the PA of charges injected in the oxide dominates the spectrum also at wavelengths shorter than 540 nm, indicating a more efficient system compared to that formed by only CdS QDs. The same conclusion can be drawn comparing this spectral region in

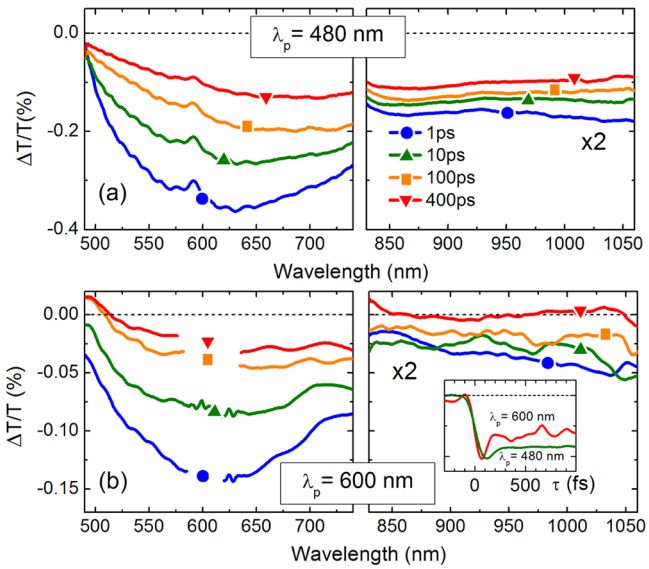

Figure 4. Transient transmission spectral evolution of the (PbS/CdS) blend deposited on TiO_2 upon excitation at 480 (a) and 600 nm (b). Signals in the NIR region have been multiplied by 2. Inset: transient transmission dynamics at 680 nm, for different pump wavelengths.

Figure 4a and b, which pumps both types of compounds or just the PbS ones. The blend sample shows a longer-lived PA signal with respect to the PbS one in the visible region (see Figure S2e, SI), denoting a lower recombination. In addition, the presence of PbS dots does not inhibit the electron transfer from CdS to the TiO_2. Finally, the PA signal has a very fast build-up time, shorter than 100 fs, irrespective of the pump wavelength (see the inset of Figure 4b for the visible and Figure S4 (SI) for the infrared probe region). This further proves the efficiency of the electron transfer. On this basis, we conclude that the blend strategy is effective and can in turn provide a route for device optimization.

DOI: 10.1021/acs.jpclett.5b00765
J. Phys. Chem. Lett. 2015, 6, 2489−2495

To confirm this analysis, we built prototype solar cells, also aiming at the optimization of the final system. We studied the functional properties of a photoelectrochemical cell composed of blended QDs, in variable percentage, on TiO_2 in contact with a suitable electrolyte for charge exchange under simulated sunlight irradiation. The counterelectrode applied in the solar cells was a nanostructured copper sulfide film prepared by spray deposition.[27]

The current density−voltage characteristic curves and the functional properties of the solar cells as a function of simulated sunlight (AM G1.5, 100 mW cm^{-2}) are shown in Figure 5.

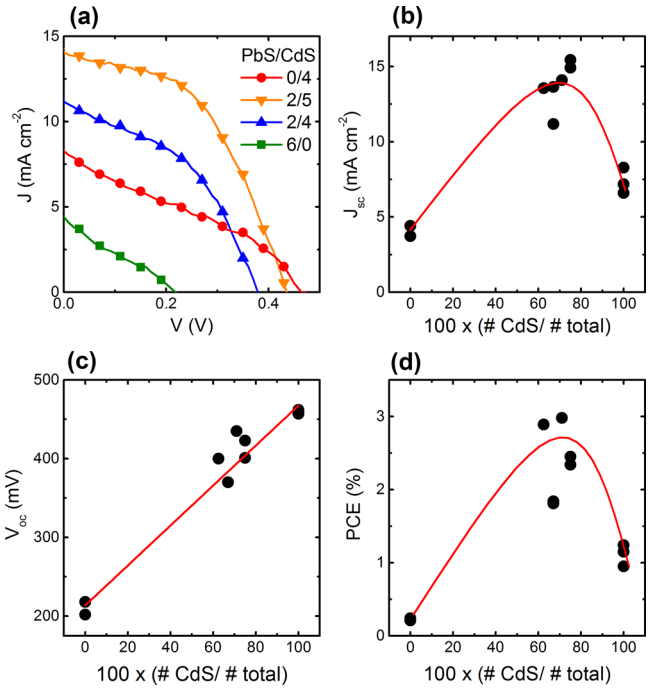

Figure 5. Functional properties of solar cells sensitized with different PbS/CdS SILAR cycles under simulated sun light at 1 sun (air mass 1.5 global, AM 1.5G, 100 mW cm^{-2}). (a) Current density versus voltage characteristic curves of selected cells. (b) Short-circuit photocurrent (J_{sc}), (c) open-circuit photovoltage (V_{oc}), and (d) PCE of photoelectrochemical cells composed of a (PbS/CdS) blend, as a function of the fraction of CdS cycles over the total number of cycles for QD growth (0 means only Pbs QDs; 100 means only CdS QDs). Red lines are a guide for the eyes.

Partial information about electron injection from QDs to TiO_2 can be deduced from the open-circuit photovoltage (V_{oc}) and short-circuit photocurrent (J_{sc}) of the solar cells fabricated using PbS, CdS, and PbS/CdS QDs. The V_{oc} is a function of electron population in the TiO_2 CB, which is determined by charge injection from the QDs; the higher the injection, the larger the population of electrons in the TiO_2 CB. For this reason, an increased V_{oc} is a clear indication of enhanced charge injection and reduced backward transfer, while in pure PbS QDs, poor exciton dissociation leads to enhanced charge recombination inside of the QD, strongly affecting the PCE of these devices.[10] As clearly seen in Figure 5, in the blended PbS/CdS QDs, V_{oc} monotonically increases with the fraction of CdS, indicating that charge injection is highly favored in the blend system (and maximized in pure CdS QDs, corresponding to 100% position in Figure 5). J_{sc} is directly related to the number of photogenerated electrons injected into TiO_2 and collected at the photoanode. The trend of J_{sc} presents a maximum for a particular (PbS/CdS) ratio, which demonstrates the effectiveness of the addition of PbS in broadening light absorption while maintaining suitable injection properties. This strategy allows one to increase the J_{sc} and the PCE by a factor of 3 and more than 10 compared to CdS and PbS simple systems, respectively. Finally, the highest PCE does not correspond to maximum light absorption but rather to a compromise between broad light absorption and effective exciton dissociation at the QD/TiO_2 interface. This result gives an important hint toward the fabrication of more efficient solar cells based on composite QDs.

In conclusion, we studied the ultrafast exciton dynamics and charge injection in composite nanocrystals grown directly on an oxide surface and demonstrated that they can be fine-tuned by modulating the QD composition and size. The photophysics of the (PbS/CdS) blend on TiO_2 and of the isolated PbS/TiO_2 and CdS/TiO_2 structures was investigated using pump−probe experiments with 100 fs time resolution. The dynamics observed in these systems enables one to understand the functional properties of the operating devices based on composite nanocrystals, in which a tailored composition of QDs leads to J_{sc} and PCE 3 times and more than 10 times higher than those of pure CdS and PbS QDs, respectively. We were able to identify the QD composition providing the best compromise between light absorption in a broad range and photogenerated charge injection to boost PCE in operating devices. These results shed light on one of the most critical processes of excitonic solar cells and pave the way to prompt significant advances in the design and fabrication of high-efficiency solar cells based on inorganic nanocrystals.

METHODS

TiO_2 Mesoporous Film Preparation. Mesoporous TiO_2 layers were prepared by tape casting a transparent layer of 20 nm sized anatase TiO_2 nanoparticles (commercial paste 18 NR-T from Dyesol) on FTO glass substrates (sheet resistance of 10 Ω/□). The layer was dried for 15 min under atmospheric conditions and then for 6 min at 120 °C before annealing at 500 °C for 30 min under an ambient atmosphere. Thickness was measured by a stylus profilometer. A single TiO_2 layer was applied for transient absorption measurements (∼5 μm thick), while a double TiO_2 layer (∼10 μm thick) was applied for solar cell fabrication and testing.

Preparation of Semiconducting QDs. Successive ionic layer absorption and reaction (SILAR) was applied to sensitize the TiO_2 photoanodes. A 0.02 M methanolic solution of Pb-$(NO_3)_2{\cdot}4H_2O$ and a 0.02 M solution of $Na_2S{\cdot}9H_2O$ in methanol/water (50/50 V/V) were used as the Pb^{2+} and S^{2-} sources, respectively, for PbS QDs. A 0.05 M ethanolic solution of $Cd(NO_3){\cdot}4H_20O$ and a 0.05 M solution of $Na_2S{\cdot}9H_2O$ in methanol/water (50/50 V/V) were used as sources of Cd^{2+} and S^{2-}, respectively, for CdS QDs. For each SILAR cycle, 1 min of dipping the TiO_2 photoanode in metallic precursor (Pb^{2+},Cd^{2+}) was applied, and then, the photoanode was washed with corresponding solvent to remove unabsorbed chemical and dried under N_2 flux. Subsequently, the same process was applied for the sulfide precursor. For deposition of composite PbS/CdS QDs, the deposition of CdS immediately followed the deposition of PbS. For this reason, we expected first the nucleation and growth of a PbS core, directly on TiO_2 surface, covered by an external CdS shell. To improve solar cell stability, a passivating ZnS capping layer was deposited by

DOI: 10.1021/acs.jpclett.5b00765
J. Phys. Chem. Lett. 2015, 6, 2489−2495

SILAR (1 cycle) after sensitization (0.1 M [$Zn(CH_3COO)_2 \cdot 2H_2O$] and 0.1 M $Na_2S \cdot 9H_20$).

Atomic Force Microscopy. AFM was performed using AppliedNano Platinum coated tips (25 nm in diameter) on QDs directly grown on highly ordered pyrolytic graphite substrates. The sample was imaged in several 1 μm × 1 μm areas. The diameters of the QDs were manually measured using dedicated software from the fwhm of the height of the dots obtained from AFM images to eliminate tip convolution effects. The cross section of the dots also confirms the same diameter convoluted by the tip diameter.

Transmission Electron Microscopy. A JEOL 2100F microscope, equipped with Oxford Instruments EDS (energy-dispersive spectroscopy), was used at 200 kV to conduct TEM analysis of samples grown on carbon films coated on TEM Cu grids. Average QD sizes were measured using image analysis of 10−15 particles for each condition.

Transient Absorption. Transient absorption measurements were carried out using the pump−probe setup shown in Figure S4a (SI). The system starts with a regeneratively amplified mode-locked Ti:sapphire laser system (Clark-MXR model CPA-1) delivering pulses with 150 fs duration at at 1 kHz repetition rate and 780 nm central wavelength. The system drives an optical parametric amplifier (OPA),[28] which generates the pump pulses for the time-resolved experiments. The OPA can be tuned in the 480−600 nm wavelength region to selectively excite the PbS and CdS quantum dots; the pulse bandwidth is 10 nm, which corresponds to a pulse duration ranging from 50 to 100 fs. For the excitation at 390 nm, pulses were produced by frequency doubling the source light; in this case, the pulse duration was 120 fs. The probe beam was a white light supercontinuum obtained by focusing a fraction of the fundamental pulse in a thin sapphire plate. The supercontinuum spectrum extends almost continuously from 460 nm to 1.6 μm, with a gap only around the fundamental wavelength at 780 nm. Acquisition in the visible or infrared spectral region was performed by selecting portions of the white light continuum by spectral filtering.

The pump beam is frequency-modulated at 500 Hz by a mechanical chopper locked to the laser pulse train. The fluence of the focused pump pulses on the samples is about 60 $\mu J/cm^2$, which corresponds to the lowest excitation providing a sufficient signal-to-noise (S/N) ratio. All experiments are performed with the same fluence to allow direct comparison of the data. Pump−probe delay is adjusted by a computer-controlled optical delay line; both pulses are then focused onto the sample. After the sample, the probe beam is selected by an iris and focused onto the entrance slit of a spectrometer equipped with electronics designed for fast read-out times and low noise,[28] allowing single-shot recording of the probe spectrum at the full 1 kHz repetition rate. By recording pump-on and pump-off probe spectra, one can calculate the differential transmission ($\Delta T/T$) (see Figure S4b of the SI) spectrum at the specific probe delay τ as

$$\frac{\Delta T}{T(\lambda, \tau)} = \frac{[T_{on}(\lambda, \tau) - T_{off}(\lambda)]}{T_{off}(\lambda)}$$

By repeating this procedure for a few hundred milliseconds and averaging the resulting signals, it is thus possible to achieve a high enough S/N ratio and to resolve $\Delta T/T$ signals as low as 10^{-4}. By moving the translation stage, we record $\Delta T/T$ spectra at different probe delays, thereby obtaining a complete 2D map, $\Delta T/T = \Delta T/T(\lambda, \tau)$. The temporal resolution of pump−probe experiments is given by the cross correlation between the pump and the (transform limit) probe duration; our system has a temporal resolution on the order of 100 fs, which is sufficient to resolve the dynamics discussed herein.

Solar Cell Fabrication and Testing. Solar cells were fabricated by sandwiching the QD-sensitized TiO_2 photoanode and a standard, highly reproducible, nanostructured copper sulfide counterelectrode using a 25 μm thick plastic spacer. Extended description of the procedure for the preparation of the copper sulfide counterelectrode is reported in detail in ref 27. Prior to cell sealing, the counter electrode was allowed to react 10 min with the polysulfide electrolyte to generate Cu_2S. Polysulfide in bidistilled water (1 M S^{2-}, 1 M S, and 0.1 M NaOH) was used as an electrolyte. The current−voltage (I−V) measurements were carried out using an ABET 2000 solar simulator under one sun simulated sunlight at AM 1.5G (100 mW cm^{-2}), calibrated with a silicon reference cell. A metallic mask with an aperture of 0.25 cm^2 was used to avoid any edge effect during the measurement.

■ ASSOCIATED CONTENT

Supporting Information

Transient transmission spectra, differential transmission dynamics, and scheme of the pump−probe experimental setup. The Supporting Information is available free of charge on the ACS Publications website at DOI: 10.1021/acs.jpclett.5b00765.

■ AUTHOR INFORMATION

Corresponding Author

*E-mail: alberto.vomiero@ltu.se

Notes

The authors declare no competing financial interest.

■ ACKNOWLEDGMENTS

A.V. is thankful to the European Union for partial salary support under contract N°299490, MC-IOF. A.V. and I.C. acknowledge the European Union for partial funding under contract N°295216, IRSES-WIROX. F.R. is grateful to NSERC for a EWR Steacie Memorial Fellowship and the Alexander von Humboldt Foundation for a FW Bessel Award and Elsevier for a grant from Applied Surface Science. G.C. acknowledges support by the European Research Council Advanced Grant STRATUS (ERC-2011-AdG No. 291198). I.C. thanks the National Research Council under the Project "Tecnologie e Materiali per l'utilizzo efficiente dell'energia solare" (Regione Lombardia). C.M. acknowledges support by MIUR FIRB grant no. RBFR12SW0J. M.Z.-R. acknowledges financial support from Fondazione Cariplo through the project NANOCRY-SLAS (grant No. 2012-0824). This work was performed in the context of the European COST Action MP1302 Nano-spectroscopy. F.R. acknowledges the FQRNT for funding through team projects, the Canada Research Chairs program for partial salary support and funding from MDEIE for an international collaboration grant in collaboration with the European Network WIROX.

■ REFERENCES

(1) Ruhle, S.; Shalom, M.; Zaban, A. Quantum-Dot-Sensitized Solar Cells. *ChemPhysChem* **2010**, *11*, 2290−2304.

DOI: 10.1021/acs.jpclett.5b00765
J. Phys. Chem. Lett. 2015, 6, 2489−2495

(2) Sambur, J. B.; Novet, T.; Parkinson, B. A. Multiple Exciton Collection in a Sensitized Photovoltaic System. *Science* **2010**, *330*, 63−66.
(3) Tisdale, W. A.; Williams, K. J.; Timp, B. A.; Norris, D. J.; Aydil, E. S.; Zhu, X. Y. Hot-Electron Transfer from Semiconductor Nanocrystals. *Science* **2010**, *328*, 1543−1547.
(4) Hyun, B. R.; Zhong, Y. W.; Bartnik, A. C.; Sun, L. F.; Abruna, H. D.; Wise, F. W.; Goodreau, J. D.; Matthews, J. R.; Leslie, T. M.; Borrelli, N. F. Electron Injection from Colloidal PbS Quantum Dots into Titanium Dioxide Nanoparticles. *ACS Nano* **2008**, *2*, 2206−2212.
(5) Wise, F. W. Lead Salt Quantum Dots: The Limit of Strong Quantum Confinement. *Acc. Chem. Res.* **2000**, *33*, 773−780.
(6) Zhao, H. G.; Fan, Z.; Liang, H.; Selopal, G. S.; Gonfa, B. A.; Jin, L.; Soudi, A.; Cui, D.; Enrichi, F.; Natile, M. M.; et al. Controlling Photoinduced Electron Transfer from PbS@CdS Core@Shell Quantum Dots to Metal Oxide Nanostructured Thin Films. *Nanoscale* **2014**, *6*, 7004−7011.
(7) Ross, R. T.; Nozik, A. J. Efficiency of Hot-Carrier Solar Energy Converters. *J. Appl. Phys.* **1982**, *53*, 6.
(8) Pijpers, J. J. H.; Koole, R.; Evers, W. H.; Houtepen, A. J.; Boehme, S.; Donega, C. D.; Vanmaekelbergh, D.; Bonn, M. Spectroscopic Studies of Electron Injection in Quantum Dot Sensitized Mesoporous Oxide Films. *J. Phys. Chem. C* **2010**, *114*, 18866−18873.
(9) Hyun, B. R.; Bartnik, A. C.; Sun, L. F.; Hanrath, T.; Wise, F. W. Control of Electron Transfer from Lead-Salt Nanocrystals to TiO_2. *Nano Lett.* **2011**, *11*, 2126−2132.
(10) Braga, A.; Giménez, S.; Concina, I.; Vomiero, A.; Mora-Seró, I. Panchromatic Sensitized Solar Cells Based on Metal Sulfide Quantum Dots Grown Directly on Nanostructured TiO_2 Electrodes. *J. Phys. Chem. Lett.* **2011**, *2*, 454−460.
(11) Lai, L.-H.; Protesescu, L.; Kovalenko, M. V.; Loi, M. A. Sensitized Solar Cells with Colloidal PbS−CdS Core−Shell Quantum Dots. *Phys. Chem. Chem. Phys.* **2014**, *16*, 736−742.
(12) Santra, P. K.; Kamat, P. V. Mn-Doped Quantum Dot Sensitized Solar Cells: A Strategy to Boost Efficiency over 5%. *J. Am. Chem. Soc.* **2012**, *134*, 2508−2511.
(13) Lee, J. W.; Son, D. Y.; Ahn, T. K.; Shin, H. W.; Kim, I. Y.; Hwang, S. J.; Ko, M. J.; Sul, S.; Han, H.; Park, N. G. Quantum-Dot-Sensitized Solar Cell with Unprecedentedly High Photocurrent. *Sci. Rep.* **2013**, *3*, 1050.
(14) Kongkanand, A.; Tvrdy, K.; Takechi, K.; Kuno, M.; Kamat, P. V. Quantum Dot Solar Cells. Tuning Photoresponse through Size and Shape Control of CdSe−TiO_2 Architecture. *J. Am. Chem. Soc.* **2008**, *130*, 4007−4015.
(15) Choi, J. J.; Lim, Y. F.; Santiago-Berrios, M. B.; Oh, M.; Hyun, B. R.; Sung, L. F.; Bartnik, A. C.; Goedhart, A.; Malliaras, G. G.; Abruna, H. D.; et al. PbSe Nanocrystal Excitonic Solar Cells. *Nano Lett.* **2009**, *9*, 3749−3755.
(16) Shalom, M.; Ruhle, S.; Hod, I.; Yahav, S.; Zaban, A. Energy Level Alignment in CdS Quantum Dot Sensitized Solar Cells Using Molecular Dipoles. *J. Am. Chem. Soc.* **2009**, *131*, 9876−9877.
(17) Tvrdy, K.; Frantsuzov, P. A.; Kamat, P. V. Photoinduced Electron Transfer from Semiconductor Quantum Dots to Metal Oxide Nanoparticles. *Proc. Natl. Acad. Sci. U.S.A.* **2011**, *108*, 29−34.
(18) Park, S.; Clark, B. L.; Keszler, D. A.; Bender, J. P.; Wager, J. F.; Reynolds, T. A.; Herman, G. S. Low-Temperature Thin-Film Deposition and Crystallization. *Science* **2002**, *297*, 65−65.
(19) Ristov, M.; Sinadinovski, G.; Grozdanov, I.; Mitreski, M. Chemical Deposition of Tin(II) Sulphide Thin Films. *Thin Solid Films* **1989**, *173*, 53−58.
(20) Li, J. J.; Wang, Y. A.; Guo, W. Z.; Keay, J. C.; Mishima, T. D.; Johnson, M. B.; Peng, X. G. Large-Scale Synthesis of Nearly Monodisperse CdSe/CdS Core/Shell Nanocrystals Using Air-Stable Reagents via Successive Ion Layer Adsorption and Reaction. *J. Am. Chem. Soc.* **2003**, *125*, 12567−12575.
(21) Zhou, N.; Chen, G. P.; Zhang, X. L.; Cheng, L. Y.; Luo, Y. H.; Li, D. M.; Meng, Q. B. Highly Efficient Pbs/Cds Co-Sensitized Solar Cells Based on Photoanodes with Hierarchical Pore Distribution. *Electrochem. Commun.* **2012**, *20*, 97−100.
(22) Gonzalez-Pedro, V.; Sima, C.; Marzari, G.; Boix, P.; Gimenez, S.; Shen, Q.; Dittrich, T.; Mora-Seró, I. n. High Performance PbS Quantum Dot Sensitized Solar Cells Exceeding 4% Efficiency: The Role of Metal Precursors in the Electron Injection and Charge Separation. *Phys. Chem. Chem. Phys.* **2013**, *15*, 13835−13843.
(23) Concina, I.; Memarian, N.; Selopal, G.; Natile, M.; Sberveglieri, G.; Vomiero, A. Spray-Assisted SILAR Deposition of Cadmium Sulphide Quantum Dots on Metal Oxide Films for Excitonic Solar Cells. *J. Power Sources* **2013**, *240*, 736−744.
(24) Concina, I.; Selopal, G. S.; Milan, R.; Sberveglieri, G.; Vomiero, A. Light Harvester Band Gap Engineering in Excitonic Solar Cells: A Case Study on Semiconducting Quantum Dots Sensitized Rainbow Solar Cells. *Pure Appl. Chem.* **2014**, *86*, 575−584.
(25) Norris, D. J.; Sacra, A.; Murray, C. B.; Bawendi, M. G. Measurement of the Size-Dependent Hole Spectrum in CdSe Quantum Dots. *Phys. Rev. Lett.* **1994**, *72*, 2612−2615.
(26) Yang, Y.; Rodriguez-Cordoba, W.; Xiang, X.; Lian, T. Strong Electronic Coupling and Ultrafast Electron Transfer between PbS Quantum Dots and TiO_2 Nanocrystalline Films. *Nano Lett.* **2012**, *12*, 303−309.
(27) Selopal, G. S.; Concina, I.; Milan, R.; Natile, M. M.; Sberveglieri, G.; Vomiero, A. Hierarchical Self-Assembled Cu_2S Nanostructures: Fast and Reproducible Spray Deposition of Effective Counter-electrodes for High Efficiency Quantum Dot Solar Cells. *Nano Energy* **2014**, *6*, 200−210.
(28) Cerullo, G.; De Silvestri, S. Ultrafast Optical Parametric Amplifiers. *Rev. Sci. Instrum.* **2003**, *74*, 1−18.

DOI: 10.1021/acs.jpclett.5b00765
J. Phys. Chem. Lett. 2015, 6, 2489−2495